Article

Optical energy variability induced by speckle: the cases of MERLIN and CHARM-F IPDA lidar

Vincent Cassé [1*], Fabien Gibert [1], Dimitri Edouart [1], Olivier Chomette [1] and Cyril Crevoisier [1]

[1] Laboratoire de Météorologie Dynamique (LMD/IPSL), École polytechnique, Institut polytechnique de Paris, Sorbonne Université, École normale supérieure, PSL Research University, CNRS, École des Ponts, F-91128 Palaiseau, France.

[*] Correspondence: vincent.casse@lmd.ens.fr

Abstract: In the context of the French-German space lidar mission MERLIN dedicated to the determination of the atmospheric methane content, an end-to-end mission simulator is being developed. In order to check whether the instrument design meets the performance requirements, simulations have to count all the sources of noise on the measurements like the optical energy variability induced by speckle. Speckle is due to interference as the lidar beam are quasi monochromatic. Speckle contribution to the error budget has to be estimated but also simulated. In this paper, the speckle theory is revisited and applied to MERLIN double pulsed IPDA lidar and also to the DLR demonstrator CHARM-F. Results show: on the signal path, speckle noise depends mainly on the size of the illuminating area on ground; on the solar flux, speckle is fully negligible both because the pixel size and the optical filter spectral width; on energy monitoring path a decorrelation mechanism is needed to reduce speckle noise on averaged data. Speckle noises for MERLIN and CHARM-F can be simulated by Gaussian noises with only one random draw by shot separately for energy monitoring and signal paths.

Keywords: speckle, coherence, interference, differential absorption lidar, radiometry, space mission

1. Introduction

Atmospheric methane is a greenhouse gas responsible for about 20% of the additional radiative forcing due to human activities since the industrial revolution [1]. In order to increase knowledge on atmospheric methane burden, the MEthane Remote LIdar missioN (MERLIN) is being developed jointly by CNES and DLR [2-4] for a scheduled launch in 2024. It plans to deliver as level 2 products: atmospheric methane total weighted columns (XCH_4) with their associated weighting functions describing the vertical sensitivity of the measurement to CH_4 variation along the atmospheric column. It targets to achieve on XCH_4 systematic (deterministic or correlated) errors less than 3 ppb and random (stochastic or uncorrelated) errors less than 22 ppb for 50 km average when the mean methane content value is 1780 ppb. That corresponds to a signal-to-noise ratio (SNR) value (the inverse of the relative random error) of 81. This challenging accuracy is needed to improve estimates of methane emissions and sinks [5] and implies to track all the sources of variability, uncertainties and biases in the measurement.

The MERLIN instruments is a double-pulsed IPDA (Integrated Path Differential Absorption) lidars [6]. The methane measurement thus relays on the Differential Atmospheric Optical Depth (DAOD) between two wavelengths. The lidar CHARM-F is an airborne demonstrator of the MERLIN instrument developed by DLR [7] that provides XCH_4 for 2 km average (7 s average as Merlin).

In the last decade, many studies have been done on the use of doubled-pulsed IPDA lidar to measure CO_2 or CH_4 atmospheric content from space [8-10] and many IPDA ground based and airborne demonstrators are been developed around the word by DLR [11-12], NASA Langley [13-20] and JPL [21-22], NIST [23-24], Tokyo Metropolitan University [25-26] or Chinese Academy of Sciences [27].

Speckle appears when coherent light is scattered by heterogeneous media at the scale of its wavelength like variations in the surface roughness or in the refractive index. Scattered waves propagate along different optical paths and interfere in any observation plan showing patterns with granular structure of alternately light and dark spots [28-29]. For IPDA lidar speckle is a serious contributor to the SNR as it induces energy fluctuations on the detector [30-39].

In this paper section 2, speckle contribution to SNR on XCH4 is pointed and with MERLIN and CHARM-F characteristics the corresponding speckle characteristics are determined. In section 3, for the two instruments, speckle noise level and shot noise level are compared for one shot and after averaging. And in section 4, a way to simulate energy fluctuations on the detector due to speckle in MERLIN simulator is described.

2. The parameters which determines the speckle contribution to XCH_4 SNR and their values for Merlin and Charm-F

2.1. How speckle contributes to signal-to-noise ratio on XCH_4 measurements ?

Double-pulsed IPDA lidar emit coherent light pulses and collect the energy scattered back by the ground surface. The atmospheric methane total weighted column (XCH_4) is estimated from the difference in atmospheric transmission between two laser pulses: one (ON) at a wavelength selected to have an high methane absorption, the other (OFF) as reference at a wavelength with significantly less methane absorption. The two pulses are close enough in wavelength and emitted with enough small interval in order to consider atmospheric, ground and instrumental optical properties to be identical except for CH_4 absorption. Nevertheless differences in H_2O and CO_2 absorption between the two beams are accounted.

From the vertical DAOD due to methane, XCH_4 is obtained as an averaged value of methane dry-air volume mixing ratio with associated weighting function WF(p)

$$XCH_4 := \frac{\int_0^{P_{surf}} XCH_4(p)WF(p)dp}{\int_0^{P_{surf}} WF(p)dp} = \frac{DAOD_{CH_4}}{\int_0^{P_{surf}} WF(p)dp} = \frac{DAOD_{slant}cos\mu - DAOD_{H_2O} - DAOD_{CO_2}}{\int_0^{P_{surf}} WF(p)dp}, \quad (1)$$

with μ the incident angle departure from nadir, and

$$WF(p) = \frac{\sigma_{CH_4}(\lambda_{on},p,T_{(p)}) - \sigma_{CH_4}(\lambda_{off},p,T_{(p)})}{g(p)\left(M_{dry} + M_{H_2O}X_{H_2O}(p)\right)}, \quad (2)$$

where σ_{CH4} is the absorption cross sections of a mole of methane depending on wavelength, pressure p and temperature T, g is the acceleration due to gravity, M_{dry} is the average molar mass of dry-air, M_{H2O} is the molar mass of water vapor and X_{H2O} is water vapor dry-air volume mixing ratio. WF(p), $DAOD_{H2O}$ and $DAOD_{CO2}$ are computed from data provided by meteorological centers and spectroscopic data found in GEISA database [40] with specific improvements [41,42].

Slant DAOD is determined as the ratio of the back-scattered energy estimates for pulses ON and OFF (P_{on} and P_{off}) normalized by emitted energy estimates for each pulse (E_{on} and E_{off}) to deal with the fluctuations of the energy delivered by the laser source [38-39].

$$DAOD_{slant} = -\frac{1}{2} ln\left(\frac{P_{on}E_{off}}{P_{off}E_{on}}\right). \quad (3)$$

The detection chain acquires these energies together with the solar flux energy P_{sun} which is also acquired on its own. The actual measurements add Gaussian noises due to random electronic noise, to shot noise and to optical energy variability on detector due to speckle. In this study, the focus is put on the speckle, the major contribution coming from the electronic chain is not studied. Comprehensive analyses of IPDA lidar noises are developed in [11,31,36].

Mean energy of scattered light by ground is space distributed according to the ground Bidirectional Reflectance Distribution Function. However for quasi monochromatic light, it fluctuates because of interference. If the light is not quasi monochromatic, interference exists for each wavelength but with a negligible effect on the spatial and temporal distribution of the total energy. For geophysical surfaces speckle pattern is fully developed. For quasi monochromatic light, relative energy fluctuations through a given aperture S during a given time T can thus be linked to the observation geometry and the wavelength through the coherence area S_c and time t_c. Signal-to-noise ratio due to speckle (SNR^{sp}) is then given by (cf. Appendix A)

$$SNR_{E/P_{xx}}^{sp} = \sqrt{\frac{2}{1+P^2}\left(1+\frac{S}{S_{c(E/P_{xx})}}\right)\left(1+\frac{T}{\tau_{c(E/P_{xx})}}\right)}, \quad (4)$$

with P characterizing the polarization of the light. In this analysis speckle due to scattering from aerosol and turbulence is not taken into account [33,35].

For an instrument, SNR^{sp} can be compared with the shot noise SNR due to the random noise relating to the photoelectric effect and to its amplification in the avalanche photo-diode used as a detector. This noise (SNR^{sn}) can be expressed as a variation of the incoming flux [11]

$$SNR_{P_{xx}}^{sn} = \sqrt{\frac{\eta N_{Pxx}}{F}}, \quad (5)$$

with N_x is the number of photons constituting the optical energy flux P_{xx}, η is the detector quantum efficiency, F is the noise factor of the avalanche photo-diode. From speckle and shot noise variability, assuming that the uncertainties are not correlated, slant DAOD uncertainty is given by

$$\sigma_{DAOD_{slant}}^2 = \frac{1}{4}\left(\left(\frac{\sigma_{P_{on}}}{P_{on}}\right)^2+\left(\frac{\sigma_{P_{off}}}{P_{off}}\right)^2+\left(\frac{\sigma_{E_{on}}}{E_{on}}\right)^2+\left(\frac{\sigma_{E_{off}}}{E_{off}}\right)^2+2(1-\alpha)\sigma_{P_{sun}}^2\left(P_{on}^{-1}-P_{off}^{-1}+E_{off}^{-1}-E_{on}^{-1}\right)^2\right), \quad (6)$$

with $\sigma_{E/P_{xx}}^2 = {\sigma_{E/P_{xx}}^{sp}}^2 + {\sigma_{E/P_{xx}}^{sn}}^2$ and α the correlation between solar flux contribution to the other measurements and its own measurement. Neglecting uncertainties coming from the integrated weighting function WF or from $DAOD_{H2O}$ and $DAOD_{CO2}$ estimates and without taking into account the full relation involving the electronic detection response function, the data sampling for ground transmission and the ground processing, the SNR for XCH_4 due to uncertainties of optical fluxes on detector (SNR^{of}) is given by

$$SNR_{X_{CH4}}^{of} = \frac{2DAOD_{CH_4}}{\sqrt{SNR_{P_{on}}^{-2}+SNR_{P_{off}}^{-2}+SNR_{E_{on}}^{-2}+SNR_{E_{off}}^{-2}+SNR_{P_{sun}}^{-2}2(1-\alpha)P_{sun}^2\left(P_{on}^{-1}-P_{off}^{-1}+E_{off}^{-1}-E_{on}^{-1}\right)^2}}. \quad (7)$$

2.2. MERLIN and CHARM-F data sets

For satellite or airborne IPDA lidar observation, the ground is counted as a plane rough surface illuminated by a coherent source and it is modeled as an extended source of chaotic light of intensity $I_C(\Delta x,\Delta y; t)$ producing a fully-developed speckle pattern resulting from interference in the propagating space (see Figure 1). The field of scattered light is observed at distance z of the rough surface and the area of coherence at this location is determined using results from Appendix A.

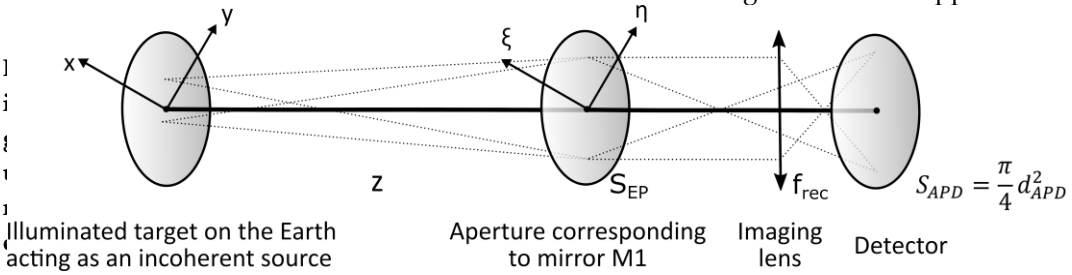

1. Observation geometry scheme.

The instrument has relative speed to ground v. It emits wavelengths in (λ_{on}) and near (λ_{off}) a methane multiplet. The emitted beam is polarized and its divergence is div_{beam}. The receiver telescope is afocal with huge magnification which image the Earth on its focal plane. The collecting mirror M1 is elliptical. To obtain a compact design, the secondary mirror M2 is close to M1, and M2 partly vignettes the entrance pupil. Up to the detector the focal length of the receiver chain is f_{rec}. A band pass filter is incorporated on the optical path to block the light outside a narrow window with size L_{filter}. The incoming signal light scattered back by the earth is focuses on the detector of diameter d_{APD} witch collect also the calibration light from the energy monitoring path [12]. That design avoids variations in the optical-to-electrical response but the energy extracted from the emitted beam has to be reduced by several orders of magnitude to match the energy level of the lidar returns. For this purpose, integrated-spheres with fiber coupling are used [38]. Cut off frequency of the electronic detection is smaller than the sampling frequency ν_{sample}. To discretise the illuminating time dependency a discretisation time δt_{dis} has to be fixed; it can be settle between a tenth of the sampling time to a sampling time.

Table 1 gives the values provided by manufacturers [6,14] for parameters which allow to compute speckle impact.

Table 1. MERLIN parameters and CHARM-F values needed to compute speckle impacts on signal

Parameter	Name	MERLIN values	CHARM-F values
Distance between ground and receiver	z	506.3 km	8.5 km
Instrument speed relative from Earth	v	7.6 km/s	0.2 km/s
ON wavelength	λ_{on}	1645.5518 nm	1645.555 nm
OFF wavelength	λ_{off}	1645.8460 nm	1645.860 nm
Polarization of the emitted beam	P	1	1
FWHM laser pulse energy density spectrum	dνl	60 MHz	50 MHz
Beam full divergence at e^{-2} at transmitter telescope output	div_{beam}	0.18125 mrad	3 to 6 mrad
Length of elliptical entrance pupil	L_{M1}	0.7325 m	0.06 m
Width of elliptical entrance pupil	l_{M1}	0.69 m	0.06 m
Obscuration of M1 by M2	O_{M2}	0.03 %	0.00 %
Focal length of reception optics	f_{rec}	0.4704 m	0.0303 m
Avalanche photo-diode diameter	d_{APD}	200 µm	200 µm
Spectral filter width	L_{filter}	2 nm	2 nm
Sampling frequency	ν_{sample}	75 MHz=1/13.3ns	100 MHz=1/10.0ns

Table 2 provides some auxiliary values computed from Table 1 parameters.

Table 2. Some geometric quantities computed from MERLIN and CHARM-F parameters

Quantity	Name	MERLIN	CHARM-F
Diameter at e^{-2} for energy distribution in the spotlight	d_{e2G}=z div_{beam}	91.8 m	25.5 to 51.0 m
Diameter of the FOV on ground	d_{fov}= z d_{APD}/f_{rec}	215.3 m	56.1 m
Effective size of the entrance pupil	$S_{EP} = \pi/4\ L_{M1}\ l_{M1}\ (1-O_{M2})$	3850.51 cm^2	28.27 cm^2

3. Speckle contributions to signal-to-noise ratio on MERLIN or CHARM-F XCH_4 measurements

Laser pulses energy is Gaussian distributed on the ground. The energy of scattered light is thus modeled as

$$I_{G(\Delta x,\Delta y)} = \frac{I_0}{2\pi\sigma_R^2} e^{\left(-\frac{1}{2}\frac{\Delta x^2+\Delta y^2}{\sigma_R{}^2}\right)}, \quad (8)$$

Preprints (www.preprints.org) | NOT PEER-REVIEWED | Posted: 26 July 2019 doi:10.20944/preprints201907.0294.v1

Peer-reviewed version available at Atmosphere 2019, 10, 540; doi:10.3390/atmos10090540

that gives by integration in the field of view (FOV) of the receiver with Eq. (A16) the effective area of the footprint looked as a secondary source for laser returns

$$S_{eff} = \frac{\left[\iint_{FOV} I_G(\Delta x,\Delta y)d\Delta x d\Delta y\right]^2}{\iint_{FOV} I_G^2(\Delta x,\Delta y)d\Delta x d\Delta y} = \frac{(2\pi\sigma_R^2)^2}{2\pi\left(\frac{\sigma_R}{\sqrt{2}}\right)^2}\frac{\left(1-e^{-\frac{1}{2}\left(\frac{r_{fov}}{\sigma_R}\right)^2}\right)^2}{1-e^{-\left(\frac{r_{fov}}{\sigma_R}\right)^2}} = 4\pi\sigma_R^2\frac{e^{\frac{1}{2}\left(\frac{r_{fov}}{\sigma_R}\right)^2}-1}{e^{\frac{1}{2}\left(\frac{r_{fov}}{\sigma_R}\right)^2}+1} \sim 4\pi\sigma_R^2 = \frac{\pi}{4}d_{e2G}^2. \quad (9)$$

Solar energy is uniform in the FOV. The energy of scattered solar flux is thus modeled by a top hat distribution

$$I_{G(\Delta x,\Delta y)}^{sun} = I_0^{sun} \text{ inside the FOV, 0 elsewhere,} \quad (10)$$

so (still using Eq. (A16)) the effective area for sun light is given by

$$S_{eff} = \frac{\pi}{4}d_{fov}^2. \quad (11)$$

Because of the movement of the satellite (or of the aircraft) during the signal energy estimation there is time speckle renewal due to changes in the illuminating of the ground at the wavelength scale[34]. With d_{eff} the characteristic size of the coherent area (the diameter for a circular area), the characteristic time of this renewal is d_{eff}/v [30] which remains considerable even for space lidar (in the order of 0.1 ms). Moreover as pulsed lidar are used, regardless of the laser beam characteristic time, there is a full coherence inside one pulse. There is no averaging of the interference pattern with increasing integration time as there is no more signal.

Table 3 provides both for MERLIN and CHARM-F the effective surface for incoherent source on ground, the coherence area; the coherence time and the number of speckles.

Table 3. Speckle characteristics for MERLIN and CHARM-F IPDA lidar (λ=1645.7 nm)

Speckle characteristics	Name	MERLIN	CHARM-F
Effective surface on ground for laser fluxes	$S_{eff}^{las} \sim \pi/4\ d_{e2G}^2$	6618.7 m²	510.7 to 2042.8 m²
Effective surface on ground for solar flux	$S_{eff}^{sun} = \pi/4\ d_{fov}^2$	36406.4 m²	2471.8 m²
Coherence surface for laser fluxes	$S_c^{las} = 4/\pi\ (\lambda/div_{beam})^2$	105 mm²	0.38 to 0.096 mm²
Coherence surface for solar flux	$S_c^{sun} = 4/\pi\ (\lambda * f_{rec}/d_{APD})^2$	19 mm²	0.079 mm²
Characteristic time for sun light	$\tau_c^{sun} = 1/(L_{filter} * c/\lambda^2)$	4.52 10^{-3} ns	4.52 10^{-3} ns
Number of spatial speckles for laser fluxes	$M_s^{las} = 1 + S_{EP}/S_c^{las}$	3668	7440 to 29449
Number of spatial speckles for solar flux	$M_s^{sun} = 1 + S_{EP}/S_c^{sun}$	20267	35786
Number of temporal speckles for laser fluxes	$M_t^{las} = 1$	1	1
Number of temporal speckles for solar flux	$M_t^{sun} = 1 + \delta t_{dis}/\tau_c^{sun}$	296 to 2951	222 to 2213

Subjective speckle for laser and solar fluxes are not to be counted as the detection optics is built in such a way that all the photons collected by the entrance pupil reach the detector. So speckle only modulates the spatial distribution of the energy on the detector and not its integrated value.

Along the optic calibration path, speckle induces fluctuations of the energy amount at each location where there is energy dilution: the output of the integrated spheres and the entrance of the optical fibers. For CHARM-F it is assumed that the detector does not truncate the fiber output [14], but for MERLIN in order to avoid alignment issues, the illuminating area is larger than the detector size. Therefore subjective speckle also occurs. For MERLIN, AIRBUS has done a dedicated study on preliminary design for this calibration path and estimated $SNR_{Eon/Eoff}$ around 43 mainly from detector and fiber entrance face [personal communication]. For CHARM-F, the $SNR_{Eon/Eoff}$ could be estimated from [38] around 59 mainly from fiber entrance face.

Table 4 summarizes SNR estimates obtained with Eq. (4) and data from Table 3 for the different fluxes in the case of MERLIN and CHARM-F. P_{on} and P_{off} are polarized, P_{sun} is not, E_{on} and E_{off} neither because integrated-spheres depolarize [44]. The maximum number of back-scattered photons for MERLIN has been estimated to less than 18000 and for CHARM-F it is about 3550 time

more (because the distance between ground and the receiver is 8.5 km instead of 506.3 km). The relative random error (RRE) is the inverse of the SNR and can be expressed in percents.

Table 4. SNR (a) and RRE (b) from speckle for MERLIN and CHARM-F lidar

	MERLIN	CHARM-F
$SNR_{PON/POFF}$	61	86
SNR_{Psun}	3470 to 10948	3986 to 12585
$SNR_{EON/EOFF}$	43	59
SNR^{sn}	< 49	about 3000

(**a**)

	MERLIN	CHARM-F
$RRE_{PON/POFF}$	1.6 %	1.2 %
RRE_{Psun}	0.0 %	0.0 %
$RRE_{EON/EOFF}$	2.3 %	1.7 %
RRE^{sn}	> 2.0 %	0.0 %

(**b**)

Speckle noise is of the same order but smaller than shot noise for MERLIN lidar. Conversely, for CHARM-F lidar, speckle noise is dominant compared to shot noise which becomes negligible with the smaller distance between the receiver and the ground.

Using a mean value of 0.53 for DAOD and a mean value of 1780 ppbv for methane content the random uncertainties coming from speckle on XCH_4 estimated with value of Table 4 and Eq. (7) are summarized in Table 5. Noise for 7s average (50 km for MERLIN, 2 km for CHARM-F)

Table 5. Random noise on XCH_4 due to speckle for MERLIN and CHARM-F lidar

	MERLIN	CHARM-F
Noise for one shot	60 ppb	41 ppb
Noise for a 7s average	5 ppb	3 ppb

The random error of 5 ppb from speckle is compatible with the specification of MERLIN random error less than 22 ppb [2] but shows how difficult it will be to reach the target user requirement for random error estimated at 8 ppb.

4. Discussion and conclusions

For satellite or airborne IPDA lidar, speckle induces variability of incident energy on the detector both for atmospheric and energy monitoring branches. SNR from speckle is estimated as above (Table 4) on a shot by shot basis. The associated noises are smaller with respect to the electronic noise for which averaging is needed. There is no difficulties to do such an average for simulated data even if geophysical variability should be taken into account to be realistic [XXX]. But the noise correlation between the various samples describing one shot and between different shots must be included.

For signal path the speckle pattern changes like the target from one shot to another. If the speckle pattern changes there is no correlation between the noises. But for energy monitoring path, the speckle pattern may be highly correlated from one shot to another. And to limit speckle impact on random noise for XCH_4 spatially averaged, it is necessary to either fully stabilize the speckle pattern, or to deliberately change it over time [45,46]. This second solution was selected for MERLIN and CHARM-F. Specific systems have been designed to change speckle pattern between successive pulses. Tests with CHARM-F showed resulting noise exhibiting pure white noise behavior which can be reduced by averaging [38]. The introduction of such a mechanism allow to have no correlation between speckle simulated noises for one shot and another [39].

Then, simulations of IPDA data with realistic speckle noise may be done taking into account the results from Table 4 and the hypothesis of full correlation for the samples of one shot (because the noise is fully correlated at this time scale as the speckle pattern is constant during the full registration of one pulse) and full decorrelation between shots.

Nothing to do for sun flux, Gaussian random noise to be added, both on each sampling of energy monitoring fluxes and on each sampling of signal fluxes, with standard deviation

respectively of 1/43 and 1/61 times the mean values, with only one random draw for energy monitoring path and signal path per shot, but a new random draw for each shot because the speckle pattern vary from one pulse to the other using the decorrelation mechanism acting between two pulses.

For the MERLIN mission, the SNR on optical energy of back-scattered signals due to speckle is around 60, always higher than the shot noise SNR which is less than 50. On contrary for CHARM-F, speckle SNR is smaller than the shot noise SNR. Subjective speckle has no impact on the energy absorbed by the detector as long as it does not truncate the energy collected. Speckle occurring on the energy monitoring path is associated to pulse by pulse SNR about 40 for MERLIN (60 for CHARM-F) and so it is the dominant speckle impact even with a decorrelation mechanism. A Gaussian model of these noises has to be included in the Merlin simulator.

Author Contributions: Conceptualization, Vincent CASSE; Resources, Fabien GIBERT and Dimitri EDOUART; Writing – original draft, Vincent CASSE; Writing – review & editing, Vincent CASSE, Fabien GIBERT, Dimitri EDOUART, Olivier CHOMETTE and Cyril CREVOISIER

Funding: This research received no external funding.

Acknowledgments: The authors acknowledge for fruitful exchanges the members of CNES MERLIN MAG. They also thank the whole bilateral MERLIN project team at CNES, DLR and AIRBUS DS.

Appendix A: Speckle theory

The speckle theory has been developed by J. C. Dainty [28] and J. W. Goodman [29] from previous studies on coherent light [47]. For any beam, its intensity (or brightness) is defined as

$$I_{(P,t)} := <u_{(P,t)} u^*_{(P,t)}>, \tag{A1}$$

and its degree of first order coherence ($g^{(1)}$) as the normalized first order correlation function between point P_1 at time t_1 and point P_2 at time t_2 [48]

$$g^{(1)}(P_1, t_1, P_2, t_2) := \frac{\langle u(P_1,t_1) u^*(P_2,t_2) \rangle}{\sqrt{I(P_1,t_1) I(P_2,t_2)}}, \tag{A2}$$

which vary between 0 for incoherent light and 1 for first order coherent light. $g^{(1)}$ is the spatial complex factor of coherence listed as $\mu(P_1,P_2)$ at a given time (t_1=t_2) and the temporal complex degree of coherence listed as $\gamma(t)$ at a given location (P_1=P_2)). It measures the visibility of interference fringes. Similarly, the beam degree of second order coherence $g^{(2)}$ is defined as the normalized second order correlation function

$$g^{(2)}(P_1, t_1, P_2, t_2) := \frac{\langle u(P_1,t_1) u^*(P_2,t_2) u^*(P_1,t_1) u(P_2,t_2) \rangle}{I(P_1,t_1) I(P_2,t_2)} = \frac{\langle I(P_1,t_1) I(P_2,t_2) \rangle}{I(P_1,t_1) I(P_2,t_2)}, \tag{A3}$$

which vary between 1 and +∞.

A monochromatic beam is said chaotic when it can be represented as a Gaussian random process [49] resulting of the well known random walk in the complex amplitude plane. Thermal light but also coherent light after fully scattering are chaotic lights. Chaotic light interferes with itself creating speckle pattern. The questions are to determine speckle sizes and the energy collected by a detector put in this speckle field.

For chaotic light, negative exponential relationship is found for the distribution of brightness

$$p\left(I_{(P,t)}\right) = \frac{1}{I_0} exp\left(-\frac{I_{(P,t)}}{I_0}\right), \tag{A4}$$

with I_0 the statistical mean value of brightness. The most probable brightness for a speckle is zero and there are more dark speckles in the field than speckles of any other brightness, but there are also rare very bright speckles.

The mean intensity of illumination W for an area S during a time ΔT results from the integration of $I_{(P;t)}$ taking into account its spatial and temporal correlations is given by

$$\overline{W} = \int_{\Delta T} \oiint_S I_{(\xi,\eta)} \, d\xi d\eta dt = I_0 \int_{\Delta T} \oiint_S g^{(1)}{}_{(\xi,\eta)} \, d\xi d\eta dt. \tag{A5}$$

Preprints (www.preprints.org) | NOT PEER-REVIEWED | Posted: 26 July 2019 doi:10.20944/preprints201907.0294.v1

Peer-reviewed version available at Atmosphere 2019, 10, 540; doi:10.3390/atmos10090540

Similarly the second-order moment is given by

$$\overline{W^2} = \int_{\Delta T} \oiint_S \int_{\Delta T} \oiint_S I_{(\xi_1,\eta_1)} I_{(\xi_2,\eta_2)} d\xi_1 d\eta_1 dt_1 d\xi_2 d\eta_2 dt_2. \quad \text{(A6)}$$

A function S(P) with values between 0 and 1 allows to take into account differences in the contribution of the various points P of the area S to the signal e.g. the sensitivity of the detector or some movement of the detector during a window time ΔT. In that last case, for a movement in the y direction the function is

$$S(x, y, t) = S(x, y - vt, 0). \quad \text{(A7)}$$

The mean value W and the standard deviation σ_W are computed using M [35, 29] defined by

$$M^{-1} := \frac{1}{\Delta T S} \int_{\Delta T} \oiint_S R_{s_{(\Delta\xi,\Delta\eta)}} \Lambda\left(\frac{\tau}{\Delta T}\right) \left(g^{(1)}_{(\Delta\xi,\Delta\eta,\tau)}\right)^2 d\Delta\xi d\Delta\eta d\tau, \quad \text{(A8)}$$

with $R_s(\Delta\xi, \Delta\eta) := \iint S(\xi, \eta) S(\xi - \Delta\xi, \eta - \Delta y) d\xi d\eta$ and Λ(x) = 1 -|x| for |x| < 1, zero otherwise.

For chaotic light, the correlation functions verify the following relation [48]

$$g^{(2)}(\Delta\xi, \Delta\eta, \tau) = 1 + \left(g^{(1)}(\Delta\xi, \Delta\eta, \tau)\right)^2, \quad \text{(A9)}$$

and then the SNR is related to M by

$$SNR = \frac{\bar{W}}{\sigma_W} = \sqrt{\frac{2}{1+P^2} M}, \quad \text{(A10)}$$

with the polarization index P (|P|=1 if the light is fully polarized, P=0 if it is not polarized). M is very well approximated as follow [29]

$$M = M_s M_t = \left(1 + \frac{S}{S_c}\right)\left(1 + \frac{T}{\tau_c}\right), \quad \text{(A11)}$$

with

$$S_c = \iint_{-\infty}^{\infty} |\mu(\Delta\xi, \Delta\eta)|^2 d\Delta\xi d\Delta\eta, \quad \text{(A12)}$$

and

$$\tau_c = \int_{-\infty}^{\infty} |\gamma(\tau)|^2 d\tau. \quad \text{(A13)}$$

Using Wiener-Khintchine and Zernike-Van Cittern theorems, τ_c and S_c may be computed from the statistics properties of the complex amplitude of the incident light. The characteristic time can be computed from the spread of its frequencies [49]. For a Gaussian beam characterized by its standard deviation σ_v, characteristic time τ_c is given by

$$\tau_c = \frac{1}{2\pi\sigma_v}, \quad \text{(A14)}$$

and for thermal light through a bandwidth filter of size L_{filter} around mean frequency λ, characteristic time τ_c is given by

$$\tau_c = \frac{cL_{filter}}{\lambda^2}. \quad \text{(A15)}$$

On a plane parallel to the emitting surface, the speckle dimensions can be computed from the brightness distribution of the emitted light on the scattering area [29]

$$S_c = (\lambda z)^2 \frac{\iint_{-\infty}^{\infty} I_G^2(\Delta x, \Delta y) d\Delta x d\Delta y}{\left[\iint_{-\infty}^{\infty} I_G(\Delta x, \Delta y) d\Delta x d\Delta y\right]^2} = \frac{(\lambda z)^2}{S_{eff}}, \quad \text{(A16)}$$

with z the distance between the source and the detector and S_{eff} the effective surface of the source corresponding to the emitting surface S in case of uniform illumination. The coherence area increases when the wave packet propagates as a result from the mix of waves coming from different points of the incoherent source. Assuming speckle and effective area are circular, the coherence area diameter is given by

Preprints (www.preprints.org) | NOT PEER-REVIEWED | Posted: 26 July 2019 doi:10.20944/preprints201907.0294.v1

Peer-reviewed version available at Atmosphere 2019, 10, 540; doi:10.3390/atmos10090540

$$d_c = \frac{4}{\pi}\frac{\lambda z}{d_{eff}} = 1.27\lambda\frac{z}{d_{eff}}. \quad \text{(A17)}$$

Further more, for a uniform illumination over a circular aperture with diameter d, Fourier transform gives the brightness distributed according to the first-order Bessel function of the first kind which first zero provides the size of coherence area

$$d_c = \frac{3.8317}{\pi}\frac{\lambda z}{d} = 1.22\lambda\frac{z}{d}. \quad \text{(A18)}$$

The small difference between factor 1.27 and factor 1.22 is generally neglected, but in the first case the full area of coherence is counted and in the second case only the disc inside the main lobe. The first approach seems more accurate for energy estimation and the second for speckle size measurements.

For completeness, speckle sizes can be estimated not only on a plane parallel to the source but also on plane with angle θ from this direction (see Figure 2).

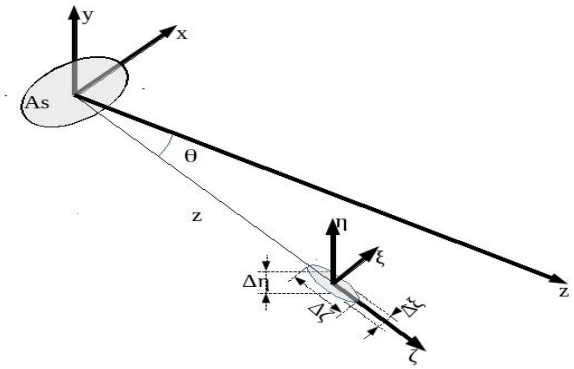

Figure 2. Speckle pattern geometry [50].

Then for an uniform source of chaotic light speckle sizes are given in the three directions by the following lengths [50]

$$\Delta\eta = 1.22\lambda\frac{z}{d}, \Delta\xi = 1.22\lambda\frac{z}{d\cos\theta}, \Delta\zeta = 8\lambda\left(\frac{z}{d}\right)^2. \quad \text{(A19)}$$

It is usual to name "objective speckle" the pattern observed on a surface due to the interference of scattered waves coming from different points of a rough surface illuminated by laser light. When such a speckle pattern is imaged using an optical system, the entrance pupil may be counted as a source of chaotic light and the interference between waves coming from different points of the imaged plane build in the image plane a new speckle pattern named "subjective speckle". The statistics properties of the scattering object determine speckle distribution in the observation plane (the area lightened). But it is the size of the entrance pupil that determines speckles dimensions (smaller is the entrance pupil, bigger are the speckles). The subjective speckle size is obtained with the same relation than above, with the numerical aperture NA instead of the one-half angular aperture

$$d_c = 1.22\frac{\lambda}{2NA}. \quad \text{(A20)}$$

So using the characteristics of a system which images the surface giving rise to the speckle: d the aperture diameter, f the focal distance and G the transverse factor of magnification, the coherence size is given by

$$d_c = 1.22\lambda\frac{(1+G)f}{d}. \quad \text{(A21)}$$

References

1. Ciais, P.; Sabine, C.; Bala, G.; Bopp, L.; Brovkin, V.; Canadell, J.; Chhabra, A.; DeFries, R.; Galloway, J.; Heimann, M.; Jones, C.; Le Quéré, C.; Myneni, R.B.; Piao, S. & Thornton, P. Carbon and Others,

Biogeochemical Cycles. In: *Climate Change 2013: The Physical Science Basis. Contribution of Working Group I to the Fifth Assessment Report of the Intergovernmental Panel on Climate Change.* Stocker, T.F.; D. Qin, G.-K. Plattner, M. Tignor, S.K. Allen, J. Boschung, A. Nauels, Y. Xia, V. Bex & P.M. Midgley (eds.). Cambridge University Press, Cambridge, United Kingdom and New York, NY, USA. **2013**, 465–570, doi: 10.1017/CBO9781107415324.015

2. Ehret, G.; Bousquet, Ph.; Pierangelo, C.; Alpers, M.; Millet, B.; Abshire, J.B.; Bovensmann, H.; Burrows, J. P.; Chevallier, F.; Ciais, P.; Crevoisier, C.; Fix, A.; Flamant, P.; Frankenberg, C.; Gibert, F.; Heim, B.; Heimann, M.; Houweling, S.; Hubberten, H.W.; Jöckel, P.; Law, K.; Löw, A.; Marshall, J.; Agusti-Panareda, A.; Payan, S.; Prigent, C.; Rairoux, P.; Sachs, T.; Scholze M. & Wirth, M. MERLIN: A French-German Space Lidar Mission Dedicated to Atmospheric Methane, *Remote Sens.* **2017**, 9, 1052-1080, doi: 10.3390/rs9101052
3. Kiemle, C.; Quatrevalet, M.; Ehret, G.; Amediek, A.; Fix, A. & Wirth, M. Sensitivity studies for a space-based methane lidar mission. *Atmos. Meas. Tech.* **2011**, 4, 2195–2211. doi: 10.5194/amt-4-2195-2011.
4. Pierangelo, C.; Millet, B.; Esteve, F.; Alpers, M.; Ehret, G.; Flamant, P.; Berthier, S.; Gibert, F.; Chomette, O.; Edouart, D.; Deniel, C.; Bousquet, P. & Chevallier F. MERLIN (Methane Remote Sensing Lidar Mission): An Overview, *ILRC 27,EPJ Web of Conferences.* **2016**, 119, 26001. doi: 10.1051/epjconf/201611926001
5. Bousquet, P.; Pierangelo, C.; Bacour, C.; Marshall, J.; Peylin, P.; Ayar, P. V.; Ehret, G.; Bréon, F.M.; Chevallier, F.; Crevoisier, C.; Gibert, F.; Rairoux, P.; Kiemle, C.; Armante, R.; Bès, C.; Cassé, V.; Chinaud, J.; Chomette, O.; Delahaye, T.; Edouart, D.; Estève, F.; Fix, A.; Friker, A.; Klonecki, A.; Wirth, M.; Alpers, M. & Millet, B. Error Budget of the MEthane Remote LIdar missioN and Its Impact on the Uncertainties of the Global Methane Budget. *JGR: Atmospheres.* **2018**, 123, 766-785. doi: 10.1029/2018JD028907
6. Bode, M.; Alpers, M.; Millet, B.; Ehret, G. & Flamant P. MERLIN: an integrated path differential absorption (IPDA) lidar for global methane remote sensing. Proc. SPIE 10563, International Conference on Space Optics - ICSO **2014** Tenerife, Canari Island, Spain. doi: 10.1117/12.2304113
7. Amediek, A.; Ehret, G.; Fix, A.; Wirth, M.; Büdenbender, C.; Quatrevalet, M.; Kiemle, C. & Gerbig, C. CHARM-F a new airborne integrated-path differential-absorption lidar for carbon dioxide and methane observations: measurement performance and quantification of strong point source emissions. *Appl. Opt.* **2017**, 56, 5182-5197. doi: 10.1364/AO.56.005182
8. Ingmann, P.; Bensi, P. & Durand, D. ESA SP-1313/1 Candidate Earth Explorer Core Missions – Reports for Assessment: A-SCOPE – Advanced Space Carbon and climate Observation of Planet Earth, Clissold P.; ESA Communication Production Office. ISBN 978-92-9221-406-7
9. Caron, J. & Durand, Y. Operating wavelengths optimization for a spaceborne lidar measuring atmospheric CO_2. *Appl. Opt.* **2009**, 48, 5413–5422. doi: 10.1364/AO.48.005413
10. NASA, Active Sensing of CO2 Emissions over Nights, Days, and Seasons (ASCENDS) Mission. NASA Science Definition and Planning Workshop Report, July 23-25, **2008**. University of Michigan in Ann Arbor, Michigan. https://cce.nasa.gov/ascends
11. Ehret, G.; Kiemle, C.; Wirth, M.; Amediek, A.; Fix, A. & Houweling S. Space-borne remote sensing of CO_2, CH_4, and N_2O by integrated path differential absorption lidar: a sensitivity analysis. *Appl. Phys. B* **2008,** 90: 593. doi: 10.1007/s00340-007-2892-3
12. Amediek, A.; Fix, A.; Wirth, M. & Ehret G. Development of an OPO system at 1.57 μm for integrated path DIAL measurement of atmospheric carbon dioxide. *Appl. Phys. B* **2008** 92: 295. doi: 10.1007/s00340-008-3075-6
13. Abshire, J.B.; Riris, H.; Allan, G.R.; Weaver, C.J.; Mao, J.; Sun, X.; Hasselbrack, W.E.; Kawa, S.R. & Biraud, S. Pulsed airborne lidar measurements of atmospheric CO2 column absorption. *Tellus B: Chemical and Physical Meteorology*, **2010**, 62, 770–783. doi: 10.1111/j.1600-0889.2010.00502.x
14. Riris, H.; Numata, K.; Li, S.; Wu, S.; Ramanathan, A.; Dawsey, M.; Mao, J.; Kawa, R. & Abshire, J.B. Airborne measurements of atmospheric methane column abundance using a pulsed integrated-path differential absorption lidar. *Appl. Opt. 2012*, 51, 8296–8305. doi: 10.1364/AO.51.008296
15. Refaat, T. F. Ismail, S. Nehrir, A. Hair, J. Crawford, J. Leifer, I. & Shuman, T. Performance evaluation of a 1.6-μm methane DIAL system from ground, aircraft and UAV platforms. *Opt. Express* **2013**, 21, 30415–30432. doi: 10.1364/OE.21.030415

16. Abshire, J.B. Ramanathan, A. Riris, H. Mao, J.; Allan, G.R.; Hasselbrack, W.E.; Weaver, C.J. & Browell, E.V. Airborne measurements of CO2 column concentration and range using a pulsed direct detection IPDA lidar. *Remote Sens*. **2014**, 6, 443–469. doi: 10.1364/AO.51.008296
17. Refaat, T. F.; Singh, U. N.; Yu, J.; Petros, M.; Ismail, S.; Kavaya, M. J. & Davis, K. J. Evaluation of an airborne triple-pulsed 2 μm IPDA lidar for simultaneous and independent atmospheric water vapor and carbon dioxide measurements. *Appl. Opt.* **2015**, 54, 1387–1398. doi: 10.1364/AO.54.001387
18. Yu, J.; Petros, M.; Singh, U. N.; Refaat, T. F.; Reithmaier, K.; Remus, R. & Johnson, W. An airborne 2-μm double-pulsed direct-detection lidar instrument for atmospheric CO2 column measurements. J. *Atmos. Ocean. Technol*. **2017**, 34, 385–400. doi: 10.1175/JTECH-D-16-0112.1
19. Singh, U. N.; Refaat, T. F.; Ismail, S.; Davis, K.; Kawa, S.R.; Menzies, R. & Petros, M. Feasibility study of a space-based high pulse energy 2 μm CO_2 IPDA lidar. *Appl. Opt.* **2017**, 56:23, 6531. doi: 10.1364/AO.56.006531
20. Abshire, J. B.; Ramanathan, A. K.; Riris, H.; Allan, G. R.; Sun, X.; Hasselbrack, W. E.; Mao, J.; Wu, S.; Chen, J.; Numata, K.; Kawa, S. R.; Yang, M. Y. M. & DiGangi, J.: Airborne measurements of CO_2 column concentrations made with a pulsed IPDA lidar using a multiple-wavelength-locked laser and HgCdTe APD detector. *Atmos. Meas. Tech.* **2018**, 11, 2001-2025, doi: 10.5194/amt-11-2001-2018
21. Wagner, G. A. &. Plusquellic, D. F. Multi-frequency differential absorption LIDAR system for remote sensing of CO2 and H2O near 1.6 μm. *Opt. Express.* 2018;,26, 19420–19434.doi: 10.1364/OE.26.019420
22. Wagner, G. A. &. Plusquellic, D. F. Ground-based, integrated path differential absorption LIDAR measurement of CO2, CH4, and H2O near 1.6 μm. *Appl. Opt.* 2016, 55, 6292–6310 .doi: 10.1364/AO.55.006292
23. Spiers, G. D.; Menzies, R. T.; Jacob, J.; Christensen, L. E.; Phillips, M. W.; Choi, Y. & Browell, E. V. Atmospheric CO2 measurements with a 2 μm airborne laser absorption spectrometer employing coherent detection. *Appl. Opt.* **2011**, 50, 2098–2111. doi: 10.1364/AO.50.002098
24. Menzies, R. T.; Spiers, G. D. & Jacob, J. C. Airborne laser absorption spectrometer measurements of atmospheric CO2 column mole fractions: source and sink detection and environmental impacts on retrievals. *J. Atmos. Ocean. Technol.* **2014**, 31, 404–421. doi: 10.1175/JTECH-D-13-00128.1
25. Sakaizawa, D.; Kawakami, S.; Nakajima, M.; Sawa, Y. & Matsueda, H. Ground-based demonstration of a CO2 remote sensor using a 1.57 μm differential laser absorption spectrometer with direct detection. *J. Appl. Remote Sens.* **2010**, 4, 043548. doi: 10.1117/1.3507092
26. Sakaizawa, D.; Kawakami, S.; Nakajima, M.; Tanaka, T.; Morino, I. & Uchino, O. An airborne amplitude-modulated 1.57 μm differential laser absorption spectrometer: simultaneous measurement of partial column- averaged dry air mixing ratio of CO2 and target range. *Atmos. Meas. Tech*. **2013**, 6, 387–396. doi: 10.5194/amt-6-387-2013
27. Du, J.; Zhu, Y.; Li, S.; Zhang, J.; Sun, Y.; Zang, H.; Liu, D.; Ma, X.; Bi, D.; Liu, J.; Zhu, X. & Chen, W. Double-pulse 1.57 μm integrated path differential absorption lidar ground validation for atmospheric carbon dioxide measurement. *Appl. Opt.* **2017**, 56, 7053–7058. doi: 10.1364/AO.56.007053
28. Dainty, J.C. Laser Speckle and Related Phenomena, Springer, **1975**. doi: 10.1007/978-3-662-43205-1
29. Goodman, J. W. Statistical Optics, John Wiley & Sons, **1985**. ISBN 978-0471399162
30. Ohtsubo, J. & Asakura, T. Velocity measurement of a diffuse object by using time-varying speckles. *Opt Quant Electron.* **1976,** 8, 523-529. doi: 10.1007/BF00620143F
31. Ostberg K. Differential absorption lidar: effects of speckle noise, FOA-report 13 No 1, 1979, National Defence Research nst. Stockholm 80, Sweden.
32. Flamant, P. H. Menzies, R.T. & Kavaya, M. J.; Evidence for speckle effects on pulsed CO_2 lidar signal returns from remote targets. Appl. Opt. **1984**, 23, 1412-1417. doi: 10.1364/AO.23.001412
33. Murty, S. R. Aerosol speckle effects on atmospheric pulsed lidar backscattered signals. *Appl. Opt.* **1989**, 28, 875-878. doi: 10.1364/AO.28.000875
34. MacKerrow E.P. & .Schmitt M.J. Measurement of integrated speckle statistics for CO2 lidar returns from a moving, nonuniform, hard target. *Appl. Opt.* **1997,** 36, 6921-6937. doi: 10.1364/AO.36.006921
35. Nelson, D. H.; Walters, D. L.; MacKerrow, E. P.; Schmitt, M. J.; Quick, C. R.; Porch, W. M. & Petrin, R. R. Wave optics simulation of atmospheric turbulence and reflective speckle effects in CO_2 lidar. *Appl. Opt.* **2000**, 39, 1857-1871, doi: 10.1364/AO.39.001857
36. Chen, J. R.; Numata, K. & Wu, S. T. Error reduction methods for integrated-path differential-absorption lidar measurements. *Opt. Express.* **2012**, 20, 15589–15609. doi: 10.1364/OE.20.015589

37. Refaat, T. F.; Singh, U. N.; Petros, M.; Remus, R. & Yu, J. Self-calibration and laser energy monitor validations for a double-pulsed 2-μm CO2 integrated path differential absorption lidar application. *Appl. Opt.* **2015**, 54, 7240–7251. doi: 10.1364/AO.54.007240
38. Fix, A.; Quatrevalet, M.; Amediek, A. & Wirth, M. Energy calibration of integrated path differential absorption lidars. *Appl. Opt.* **2018**, 57, 7501-7514. doi: 10.1364/AO.57.007501
39. Wenyi H.; Jiqiao L.; Yadan Z.; Junfa D.; Xiuhua M.; Shiguang L.; Junxuan Z.; Xiaopeng Z. & Weibiao C. Analysis of energy monitoring for a double-pulsed CO_2 integrated path differential absorption lidar at 1.57 μm. *Appl. Opt.* **2019;** 58, 616-625. doi: 10.1364/AO.58.000616
40. Jacquinet-Husson, N.; Armante, R.; Scott, N.A.; Chedin, A.; Crépeau, L.; Boutammine, C.; Bouhdaoui, A.; Crevoisier, C.; Capelle, V.; Boonne, C.; Poulet-Crovisier, N.; Barbe, A.; Chris Benner, D.; Boudon, V.; Brown, L.R.; Buldyreva, J.; Campargue, A.; Coudert, L.H.; Devi, V.M.; Down, M.J.; Drouin, B.J.; Fayt, A.; Fittschen, C.; Flaud , J.M.; Gamache, R.R.; Harrison, J.J.; Hill, C.; Hodnebrog, Ø.; Hu, S.M.; Jacquemart, D.; Jolly, A.; Jimenez, E.; Lavrentieva, N.N.; Liu, A.W.; Lodi, L.; Lyulin, O.M.; Massie, S.T.; Mikhailenko, S.; Müller, H. S. P.; Naumenko, O.V.; Nikitin, A.; Nielsen, C.J.; Orphal, J.; Perevalov, V.I.; Perrin, A.; Polovtseva, E.; Predoi-Cross, A.; Rotger, M.; Ruth, A.A.; Yu, S.S.; Sung, K.; Tashkun, S.A.; Tennyson, J.; Tyuterev, VI.G.; Vander Auwera, J.; Voronin, B.A. & Makie, A. The 2015 edition of the GEISA spectroscopic database. *J. Mol. Spectrosc.* **2016**, 327, 31-72, doi: 10.1016/j.jms.2016.06.007
41. Delahaye, T.; Maxwell, S. E.; Reed, Z. D.; Lin, H.; Hodges, J. T.; Sung, K.; Devi, V.; Warneke, T. & Tran, H. Precise methane absorption measurements in the 1.64 μm spectral region for the MERLIN mission. *JGR. Atmospheres.* **2016**, 121, 7360–7370. doi: 10.1002/2016JD025024
42. Delahaye, T.; Ghysels, M.; Hodges, J. T.; Sung, K.; Armante, R. & Tran, H. Measurement and modeling of air-broadened methane absorption in the MERLIN spectral region at low temperatures. *JGR Atmospheres.* **2019**, 124, 3556– 3564. doi: 10.1029/2018JD028917
43. Tellier, Y.; Pierangelo, C.; Wirth, M.; Gibert, F. & Marnas, F. Averaging bias correction for the future space-borne methane IPDA lidar mission MERLIN. *Atmos. Meas. Tech.* **2018**, 11, 5865-5884, doi: 10.5194/amt-11-5865-2018
44. McClain, S. C.; Bartlett, C. L.; Pezzaniti, J.L. & Chipman, R. A. Depolarization measurements of an integrating sphere. *Appl. Opt.* **1995**, 34, 152-154. doi: 10.1364/AO.34.000152
45. Lowenthal, S. & Joyeux, D. Speckle Removal by a Slowly Moving Diffuser Associated with a Motionless Diffuser. *J. Opt. Soc. Am*. **1971**, 61, 847-851, doi: 10.1364/JOSA.61.000847
46. Singh Mehta, D.; Naik, D.; Singh, R. & Takeda, M. Laser speckle reduction by multimode optical fiber bundle with combined temporal, spatial, and angular diversity. *Appl. Opt.* **2012**, 51, 1894-904. doi: 10.1364/AO.51.001894
47. Mandel, L. & Wolf, E. Coherence Properties of Optical Fields. *Rev. Mod. Phys.* **1965**, 37, 231-287. doi: 10.1103/RevModPhys.37.231
48. Loudon, R. The Quantum Theory of Light, *Oxford University Press*, **2000**. ISBN 0-19-850177-3
49. Wang, Q. Discussion on the fully developed speckle field. *Optik.* **2013**, 124, 2948–2950. doi: 10.1016/j.ijleo.2012.09.046
50. Li, Q. & Chiang, F. Three-dimensional dimension of laser speckle. *Appl. Opt.* **1992**, 31, 6287-6291. doi: 10.1364/AO.31.006287